

Landslides (2024) 21:309–325  
 DOI 10.1007/s10346-023-02179-4  
 Received: 20 May 2023  
 Accepted: 10 November 2023  
 Published online: 19 December 2023  
 © This is a U.S. Government work  
 and not under copyright protection  
 in the US; foreign copyright  
 protection may apply 2023

Kate E. Allstadt  · Jeffrey A. Coe · Elaine A. Collins · Francis K. Rengers ·  
 Anne Mangeney · Scott M. Esser · Jana Pursley · William L. Yeck · John J. Bellini ·  
 Lance R. Brady



## The 2022 Chaos Canyon landslide in Colorado: Insights revealed by seismic analysis, field investigations, and remote sensing

**Abstract** An unusual, high-alpine, rapid debris slide originating in ice-rich debris occurred on June 28, 2022, at 16:33:16 MDT at the head of Chaos Canyon, a formerly glacier-covered valley in Rocky Mountain National Park, CO, USA. In this study, we integrate eyewitness videos and seismic records of the event with meteorological data, field observations, pre- and post-event satellite imagery, and uncrewed aircraft vehicle imagery to characterize the event and future hazards it may pose. Deformation of the eventual slide mass preceded rapid failure by decades, starting in the early to mid-2000s, accelerating in 2018 (the warmest year on record), and reaching ~ 20 m/year in 2021. The main event, which was preceded by smaller sliding episodes earlier that day, had a volume of ~ 2.1 million m<sup>3</sup>, reached peak velocities of about 5 m/s, slid on a surface up to 80 m deep, and moved up to ~ 245 m downslope in < 2 min. We observed blocks of frozen debris (permafrost) in the landslide deposits. Within ~ 2 weeks, these blocks had melted and became dry, conical debris mounds (molards). We hypothesize that the rapid slide was induced by gradually increasing long-term air temperatures that thawed ice and increased pore pressures. The presence and suspected influence of permafrost on the occurrence of this landslide indicate other slopes in the park, and other moderate-to-low latitude alpine regions may experience similar slope stability issues as temperatures continue to warm.

**Keywords** Alpine · Debris slide · Permafrost · Climate change · Molard · Runout

### Introduction

Starting around 4:30 p.m. local time (22:30 UTC) on June 28, 2022, a steep mass of ice-rich glacial debris partly mantled with a snowfield began to mobilize from the southeast flank of Hallett Peak in upper Chaos Canyon in Rocky Mountain National Park, CO, USA (Figs. 1 and 2). The area is remote: there are no trails in the canyon and access requires a challenging scramble through an expanse of large boulders. However, people are commonly in the canyon because it is a popular climbing and bouldering destination. On the day of the slide, as slide activity began to build, several park visitors were climbing near Colossal Boulder (Fig. 1), against which the eventual landslide came to a stop. One of the climbers collected video footage of the slope moving towards them as it initially began to mobilize (Mondragon 2022). The climbers then fled when the slide started picking up speed and a dust cloud enveloped them (J. Fullerton, oral comm. 2023). They narrowly escaped without injury

(Chen 2022), and no other injuries were reported (Patterson 2022). Another eyewitness who was near Lake Haiyaha (Fig. 1) captured video of this part of the failure sequence in profile view, showing the entire slope moving relatively rapidly and coherently downslope and then becoming enveloped in dust (9news.com 2022). Energetic parts of the failure sequence generated seismic waves that were picked up on seismic stations up to about 70 km away.

Following the event, the US National Park Service (NPS) closed all of Chaos Canyon west of Lake Haiyaha to the public (Patterson 2022), and at the time of publication, this closure remained in effect. The NPS requested technical assistance from the US Geological Survey (USGS), so three of the authors of this article, accompanied by NPS climbing rangers, visited the landslide on foot on July 15, 2022, to collect data and make observations to characterize the event. In particular, NPS was interested in information about possible ongoing hazards to help inform their decision making.

The landslide, referred to as the Chaos Canyon landslide, occurred in colluvial and glacial deposits in a high alpine landscape. Recent modeling and mapping indicate a high likelihood that the slope could contain permafrost (Janke 2005a; Achuff 2001). The effect of warming temperatures on formerly glacier-covered (glaciated) alpine landscapes is an ongoing research topic (e.g., Haerberli et al. 1997; Allen et al. 2009; Patton et al. 2019; Penna et al. 2023), partly because of uncertainty about ice (i.e., permafrost) remaining in glacial deposits, talus, rock glaciers, and bedrock. Potential effects on landslide occurrence are especially relevant, particularly in areas frequently visited by people, such as parks. Based on a literature search, large, catastrophic landslides (very to extremely rapid failures with velocities > 3 m/minute (IUSS 1995)) originating in ice-rich debris or rock glaciers in glaciated landscapes are apparently rare, perhaps because few people visit these areas so that they largely go unnoticed. The few cases we found that were most similar were two debris slides and avalanches sourced in frozen debris in Iceland and Greenland (Sæmundsson et al. 2018; Morino et al. 2019; Svennevig et al. 2022) and two partial collapses of rock glaciers in the Alps and Andes (Bodin et al. 2012, 2017).

In this paper, we provide insights into landslides in post-glacial alpine environments by investigating this unusual event and the circumstances under which it occurred. We present an analysis of the Chaos Canyon landslide based on field and remotely sensed observations, including mapping from high resolution imagery collected by uncrewed aerial vehicle (UAV), satellite imagery, pre- and post-event topographic data, eyewitness reports, meteorological

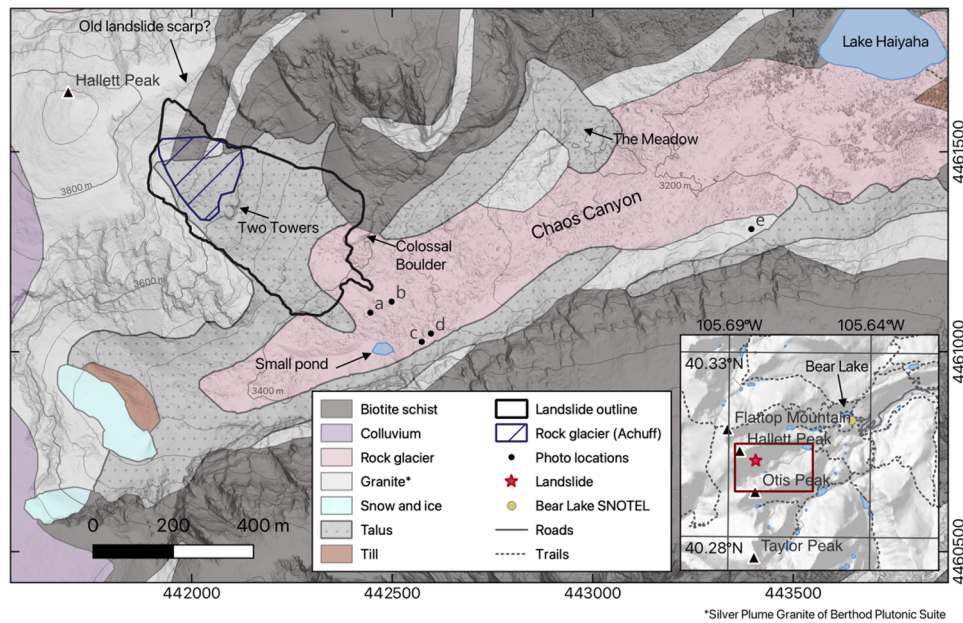


**Fig. 1** Geologic setting of Chaos Canyon landslide and landmarks mentioned in text overlain on pre-event (2020) 1-m lidar digital elevation model with 50-m contour lines. Underlying geologic map from Braddock and Cole (1990), blue hashed area indicates the approximate portion of the source area mapped as a “rock glacier or debris-covered glacier” by Achuff (2001). Black dots indicate photo locations mentioned later in the text. Inset map shows the location of the main panel (red outline) relative to Rocky Mountain National Park geography. Base data from <https://romo-nps.opendata.arcgis.com/datasets>. Coordinate reference system NAD83(2011)/UTM zone 13N

data, and seismic records of the event. We end with a discussion of potential ongoing hazards and implications for similar slopes in glaciated alpine settings.

### Background

Chaos Canyon is a glaciated ~2-km-long U-shaped valley just east of the Continental Divide carved out of metamorphic and intrusive igneous rocks, specifically Early Proterozoic biotite schist and Middle Proterozoic Silver Plume Granite of Berthoud Plutonic Suite (Braddock and Cole 1990) (Fig. 1). The mouth of the canyon, at Lake Haiyaha, is at an elevation of about 3115 m. The landslide source area is ~1.5 km up the canyon and spans an elevation of about 3460 to 3760 m. Covering the floor of the valley and forming part of the runout path of the landslide is the Chaos Canyon rock glacier (Fig. 1), an inactive or relic tongue-shaped rock glacier (White 1976; Achuff 2001; Janke 2007) with possible landslide origins (Colton et al. 1976). This rock glacier is dated to about 5000 to 3865 years before present (Richmond 1960; Madole 1976) although possibly older (Davis 1988), and is composed at the surface primarily of extremely large boulders reaching 5 to 15 m in the longest dimension. Water flows mainly below the boulders into Lake Haiyaha, and there is no clear surface channel. With the exception of lichens, the boulder-strewn terrain of the floor of the canyon supports little vegetation (Madole 1976). Isolated pockets of subalpine to alpine tundra exist in depressions around the edges of the rock glacier and up the sides of the canyon in some areas. Essentially no vegetation is visible in satellite imagery in the landslide source area.

The canyon is flanked on all sides by steep bedrock and talus slopes (Braddock and Cole 1990) (Fig. 1). The source area of the

landslide was mapped as a ~400-m-long wedge of talus above and directly adjacent to (and possibly overlying part of) the Chaos Canyon rock glacier. Much of the talus in similar settings in the region, high up in valley heads, is thought to be associated with the two younger stages of Holocene glaciation, especially the Audubon advance (~1850–950 years B.P.) (Madole 1976), but also, to a lesser extent, the Arapaho Peak advance during the Little Ice Age (~350–100 years B.P.) (Janke 2005b).

The landslide source area lies immediately downslope from a cirque with a steep granite headwall. Northeast-facing cirques at similar elevations in adjacent valleys, including the southern spur of Chaos Canyon, are occupied by small glaciers or glacierets (Hoffman et al. 2007), some of which grade into active ice-cored rock glaciers (Janke 2005b). However, the landslide source area does not share this characteristic, perhaps in part due to its more southeasterly aspect (~110°). Instead, at the base of the headwall, at about 3700 m elevation, where bedrock meets the debris, is a snowfield that was once perennial (Achuff 2001) but Landsat Level-1 imagery indicates has melted completely by the end of some recent summers (at least early Fall 2015, 2018, 2021; USGS 2022a). Snow accumulation is likely driven by avalanches and westerly winds that blow snow from the penneplain above, into eastern-facing cirques (Lee 1923; Hoffman et al. 2007; Janke and Frauenfelder 2008; McGrath 2022). Mean annual precipitation at Bear Lake SNOTEL station ([www.wcc.nrcs.usda.gov/snow/](http://www.wcc.nrcs.usda.gov/snow/)), located ~3.2 km northeast of the landslide at an elevation of ~2900 m (Fig. 2) from 2006 to 2022 was 93 cm (~20 cm of snow water equivalent). The mean annual temperature for water years 1990–2022 at Bear Lake was 3.3 °C. Adjusting this value to

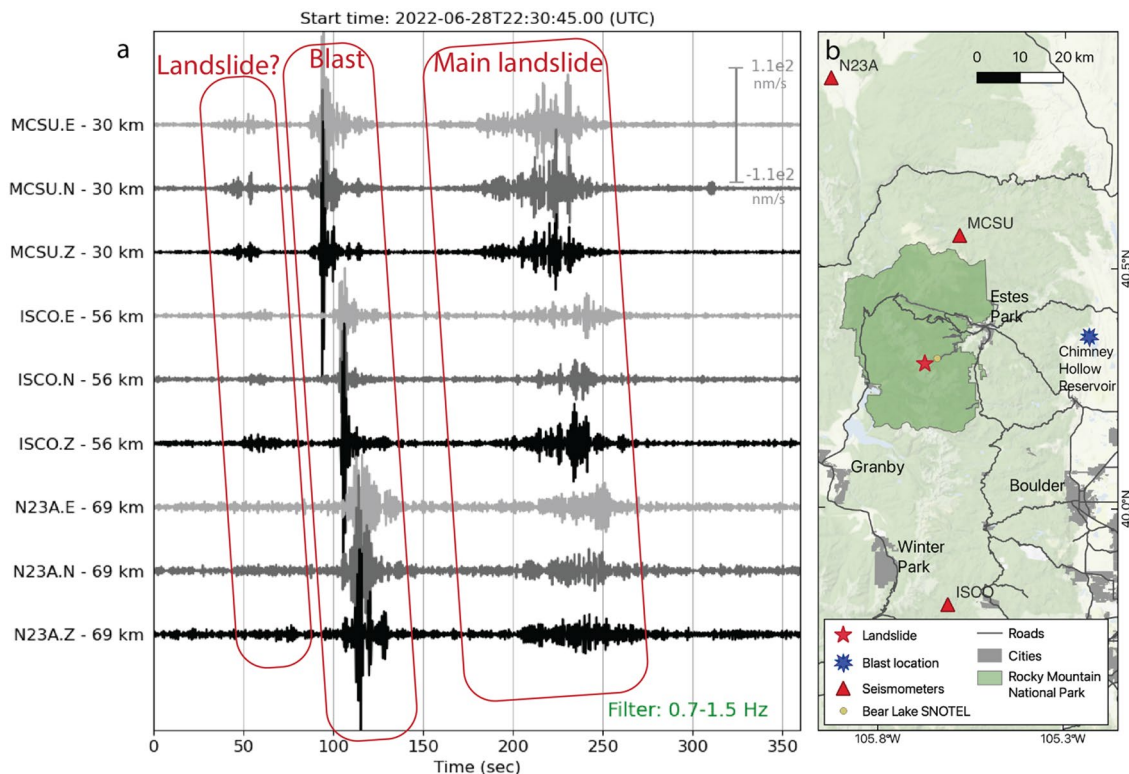


**Fig. 2** Seismic signals of the sequence of events (a) and associated map of event locations and seismic stations (b) described in the main text. The zero time corresponds to 22:30:45 UTC (4:30:45 p.m. MDT). Seismic signals are corrected to ground velocity, filtered in a narrow band (0.7-1.5 Hz) to suppress local noise on station MCSU, and all plotted on the same amplitude scale (scale bar at right). Labels at left indicate the seismic station name, component (E-East, N-North, Z-vertical), and distance from the landslide. MCSU and N23A are operated by the Colorado Geological Survey Seismic Network (network code C0) (Colorado Geological Survey 2016), and ISCO is part of the US National Seismic Network (network code US) (Albuquerque Seismological Laboratory (ASL)/USGS 1990). Base data map data from <https://romo-nps.opendata.arcgis.com/datasets> and <https://data.colorado.gov>. Coordinate reference system WGS84

the elevation of the center of the landslide of 3600 m using a 0.5 °C/100 m mountain adiabatic lapse rate (Janke 2005c) yields a mean annual temperature estimate of -0.2 °C. These mean temperatures near zero raise the question of whether debris in the landslide source area contains permafrost (interstitial or an ice core). Permafrost modeling of the Front Range estimated that the landslide source area had a 76–100% probability of containing permafrost (Janke 2005a).

If the slope did contain permafrost, given that the area was formerly glacier-covered and neighboring valleys contain active rock glaciers, this also leads to the question of whether the slope could be considered a rock glacier. This would be the case if it moved by creep due to ice deformation. The upper portion of the source area was mapped as a rock glacier by Achuff (2001) (Fig. 1), but other work in the area does not identify it as a rock glacier (Braddock and Cole 1990; Janke 2007). If the landslide source was a rock glacier, it is not typical of those in the region in morphology or aspect (e.g., Outcalt and Benedict 1965; White 1976; Janke 2007; Janke and Frauenfelder 2008). The slope has a lumpy surface, but it does not have obvious flow indicators, such as ridges or furrows. The landslide slope does, however, have a steep frontal slope with a sharp junction angle typical of rock glaciers (e.g., Janke 2007), and, like

many rock glaciers, the landslide slope is fed debris and snow by a cirque headwall.

### Recent landslide history in the area

Landslides in the southern Rocky Mountain region are most often triggered by snowmelt or rainfall (Anderson et al. 1984; Chleborad 1998; Cannon et al. 2003; Coe et al. 2014). In a few unusual, but noteworthy cases, landslides have been triggered by earthquakes (e.g., Hadley 1964) or by rain-on-snow events (e.g., Coe et al. 2016). Whether or not landslides are triggered by degradation of in situ ice (e.g., mountain permafrost or rock glacier cores) is an open question for glaciated, high-altitude parts of the southern Rocky Mountains. However, degradation of ice is an important landslide triggering factor in other parts of the world (e.g., Haeberli et al. 1997; Raveland and Deline 2011; Sæmundsson et al. 2018; Patton et al. 2019; Penna et al. 2023).

One of the best-known examples of snowmelt triggered landslides in the region occurred in Utah in the spring of 1983 where winter snowpack was 150–400% above normal (Anderson et al. 1984), and a sustained period of high temperatures, caused widespread snowmelt-induced debris flows (Wieczorek et al. 1989)

and the Thistle landslide (Duncan et al. 1986). The Thistle landslide resulted in the relocation of a highway and a railroad. Total costs (direct and indirect) from the landslide were about \$400 million (in 1984 dollars), which likely makes it the costliest single landslide in US history (Schuster and Highland 2001).

For rainfall triggered landslides, two of the best recent examples are from high alpine areas in the Colorado Front Range. In July 1999, about 60 km south of Chaos Canyon, an intense afternoon thunderstorm triggered ~ 480 debris flows along the Continental Divide (Godt and Coe 2007). In September 2013, prolonged rainfall triggered more than 1100 debris flows in the northern Front Range in areas that were preferentially low in vegetation density (Rengers et al. 2016), including about 25 within Rocky Mountain National Park (Coe et al. 2014).

## Methods

### Digital elevation model and volume estimates

We used a DJI Mavic Pro Uncrewed Aerial Vehicle (UAV) to image the landslide on July 15, 2022. Still photos were georeferenced using an onboard global positioning system, and subsequently used to create a Structure from Motion (SfM) point cloud and orthophoto using Agisoft Metashape (Agisoft 2022). Because of the hazard of the slide area, we were not able to place control points on the ground. As a result, we performed additional corrections to better align the post-event point cloud to the pre-event topography. To do so, we used the CloudCompare software (EDF R&D 2023) to align the post-event point cloud to a digital elevation model (DEM) derived from a 1-m pre-event airborne lidar flown in 2020 (USGS 2022b) using manually picked point pairs on landmarks in unchanged areas around the edges of the landslide. The mean vertical difference in unchanged areas was 0.69 m, and the standard deviation was 2.5 m. The post-event DEM, high-resolution orthophoto, and original UAV images are available in Rengers et al. (2023).

To estimate the total landslide volume, we had to estimate the location of the sliding plane because the landslide deposits did not completely evacuate the source area. We did this by fitting 18 logarithmic spiral profiles 20-m apart between the part of the source area that was void of deposits from the post-event DEM, and the surface of the pre-event slope below the source area. We also used linear interpolation for the profiles as an alternate lower-bound model. We next interpolated and smoothed a piecewise-linear three-dimensional (3D) function between these profiles and the surrounding topography to obtain a DEM of the sliding surface. We then differenced this surface from both the pre- and the post-event DEMs, multiplied by the area of each cell (1 m<sup>2</sup>), and summed over the area of the landslide to estimate the source area volume and deposit volume separately. We estimated the uncertainties of the total volume estimates due to DEM errors by using standard uncertainty propagation methods for linear combinations with spatial correlation. We assumed a constant standard deviation of 2.5 m, estimated above, and quantified the spatial correlation of differences between the pre- and post-DEM in stable areas as described in Online Resources 1 to construct the covariance matrix needed for this uncertainty estimation.

### Seismic methods

The seismic signals associated with the landslide were not detected automatically by routine seismic monitoring networks because the signals were weak. Also, earthquake detection and location algorithms are generally not effective for landslide seismic signals. We instead searched manually for signals on nearby stations (Fig. 2b) that occurred around the time of the eyewitness reports. We searched for signals that had landslide characteristics (more emergent onsets, lower frequencies than earthquake signals (e.g., Allstadt et al. 2018)) and relative station arrival times consistent with the landslide location. We estimated these times using seismic velocities for shallow propagating S-waves and surface waves of about ~ 3 km/s (Herrmann et al. 2011). We estimated the start time of each landslide event by correcting the time that the signal emerged from the noise on each seismic station for travel time using ~ 3 km/s, and then, we took the earliest of those estimates as the approximate start time. The seismic signals associated with the June 28, 2022, landslide sequence are fairly low-amplitude and narrowband compared to other larger rapid, catastrophic landslides. Therefore, other than for event timing, we were mainly limited to qualitative interpretations of the signals such as approximate event durations, and relative changes in energy over time.

### Deformation prior to the 28 June 2022 landslide

We were able to track deformation for decades prior to the June 28 landslide using simple techniques because of the presence of two blocky building-sized rocks (each about 25 m wide) embedded in the landslide slope at about 3600 m elevation. These rocks are informally referred to as the “Two Towers” (Fig. 1). Prior to June 28, the Two Towers were located at a slope change. Upslope from the Two Towers, which was the part of the landslide source area previously mapped as a rock glacier (Achuff 2001), the average slope was 30°, and the surface was notably coarser and lumpier than the area downslope from the towers. The area downslope from the towers (herein called the frontal slope) was steeper, with an average slope of about 40°. It was lighter gray in color and finer grained than the upslope area, with a few embedded larger boulders (Fig. 3a). Large boulders were concentrated at the bottom of the slope, and one of the eyewitnesses who frequently climbed in the area mentioned that he saw large boulders rolling down the frontal slope on occasion in the past (J. Fullerton, oral comm. 2023; Butzer 2022). In some pre-event imagery, dozens of springs are visible coming from this frontal slope at a range of elevations (Fig. 3b). Some spring locations are persistent between years, and at least one rill downslope from a spring is lined by levees indicating that small debris flows may have originated in the area of some of the springs in the past.

When we investigated the available pre-event imagery, we noticed that downslope movement of tens of meters was clearly visible over the years. This was especially obvious when looking at the Two Towers, but also was notable in the eventual headscarp area where tensile fractures in the vicinity started visibly widening after 2016 (Fig. 3). We investigated this deformation systematically by tracking the centroid of the polygon outlining the Two Towers using 13 orthorectified aerial and satellite images from Planet Labs, Maxar, and USGS Earth Explorer from 1990 to 2022 (Fig. 3; Online Resources

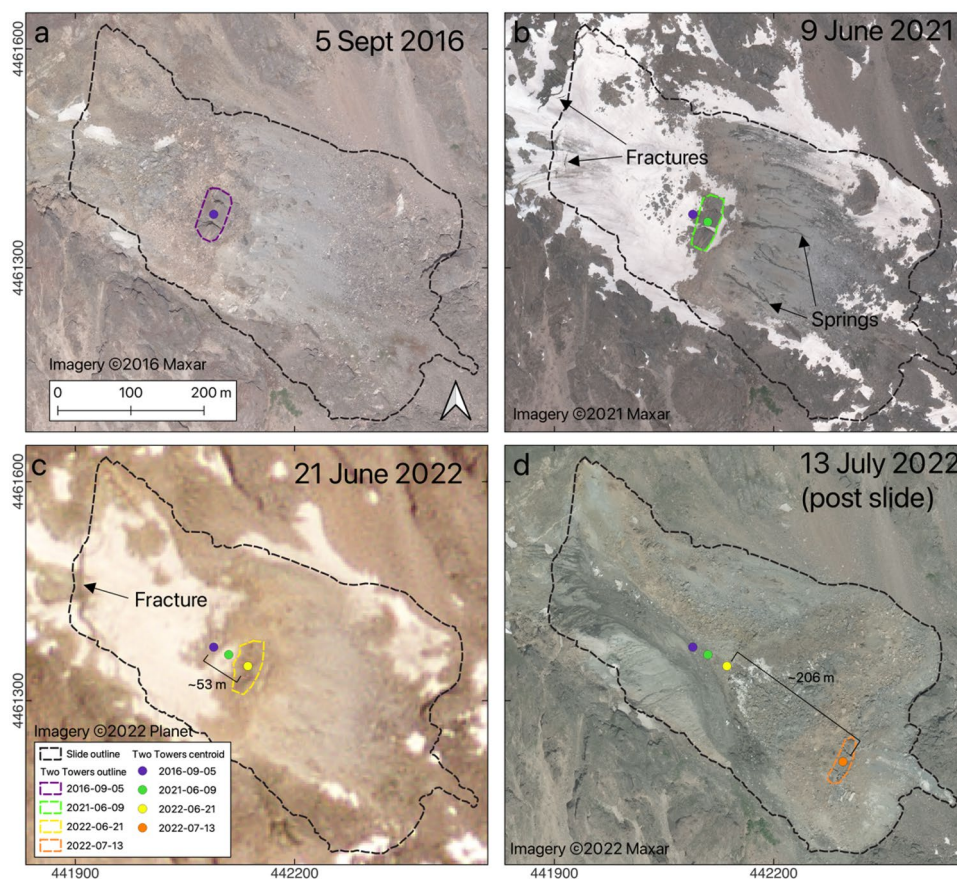


**Fig. 3** Satellite imagery showing the evolution of the landslide and movement of the centroid and polygon outline of the informally named “Two Towers.” **a** The landslide nearly snow-free in Sept 2016. **b** The first known appearance of the tensile fractures in the snowfield in June 2021, also showing numerous springs originating from the frontal slope. **c** The closest pre-event imagery to the failure date (lower resolution), from June 2022, showing the fracture widening. **d** The first cloud-free high-resolution post-landslide image (15 days post-event). Values shown in **c** and **d** are horizontal distances. Coordinate reference system NAD83(2011)/UTM zone 13N

1 Fig. S3). We only used images that were well-orthorectified based on the stability of features outside the landslide mass. We found that the landslide started to move substantially sometime between 2000 and 2009 and that cumulative horizontal movement of the Two Towers prior to June 2022 was more than 60 m (Fig. 4a; ~73 m slope-parallel). The tensile fractures became one main ~200-m long continuous fracture by early 2022 and widened to 5–8 m by the time of the last pre-event image, which was taken about a week prior to the landslide (Fig. 3c; Online Resource 1 Fig. S8a–c). This fracture ultimately formed the western bound of the scarp of the landslide (Fig. 3d; Online Resource 1 Fig. S8d).

Increasing deformation rates appear to be positively correlated with increasing average annual temperatures (Fig. 4a, b). Annual mean temperatures in the area have been on a clear upward trajectory since the 1990s. The annual mean temperature at the elevation of the center of the landslide (~3600 m), estimated by adjusting the data from the nearby Bear Lake SNOTEL station for elevation (using 0.5 °C/100 m in elevation, Janke (2005c)), started to regularly exceed 0 °C starting in about 2006 (Fig. 4b), during the same period when landslide movement began. The slide deformation rate accelerated after 2018, which also was the warmest year on record (Fig. 4a, b).

The weather immediately prior to the landslide, however, was not anomalous for alpine areas in Colorado. The spring melt was well underway. Daily mean temperatures roughly followed the long-term trend (Fig. 4c) and exceeded 0 °C nearly every day after early May. Deviations from the trend included two cold, snowy periods in the second half of May, followed by a 5-day stretch in the second week of June where temperatures were 3–8 °C warmer than average. Temperatures for 2 weeks prior to the landslide were generally oscillating within a few degrees of the long-term average. About 0.8 cm of precipitation, likely falling as rain given the warm temperatures, fell 2 days prior to landslide.

### The 28 June 2022 landslide

#### Timeline

We reconstructed a timeline of the series of events on the day of the main landslide based on eyewitness accounts, videos, and seismic records. This combination of data provides a detailed story of how the event unfolded that is rarely available for natural events. We interviewed one of the eyewitnesses who was climbing in the area when the landslide occurred, and we obtained other eyewitness

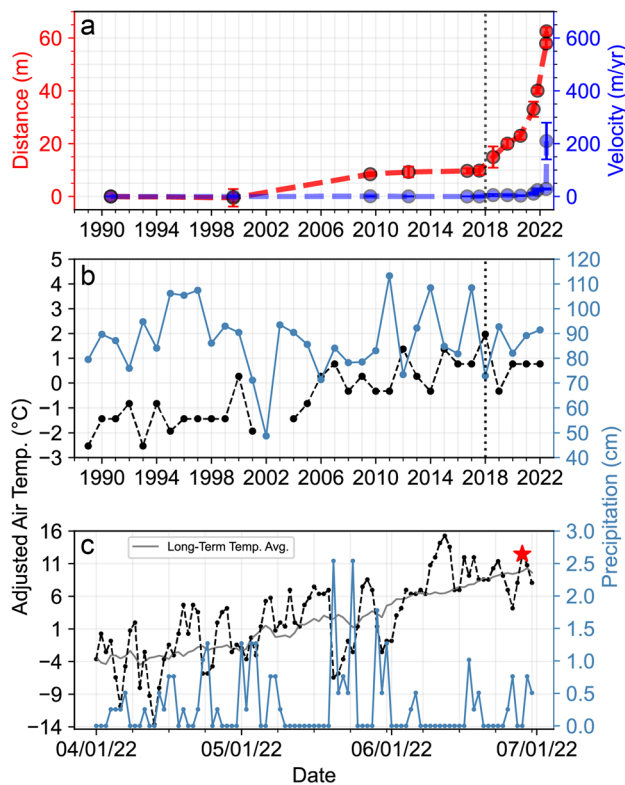


**Fig. 4** Displacements of the informally named “Two Towers” prior to the 28 June 2022 event compared with temperature and precipitation recorded at the Bear Lake (322) SNOTEL weather station (elevation 2902 m). All temperatures are adjusted for adiabatic-lapse-rate to the elevation of the center of the slide (3627 m). **a** Two Towers horizontal (map-view) displacement distance and velocity through 21 June 2022, relative to 27 August 1990. Uncertainties (as shown by the error bars) are estimated by the farthest distance from the “best” polygon centroid to centroids of sets of alternate reasonable polygons. **b** Annual mean air temperature (black) and annual total precipitation (blue) for water years 1990–2022. No annual mean air temperature is published for water years 2002, 2003, and 2021 due to too many missing days of data. We estimated the value for 2021 using available data. Dotted, vertical black line indicates when the landslide began accelerating and also the warmest year on record. **c** Daily precipitation total (blue) and daily mean temperature (black) recorded at Bear Lake SNOTEL in the 3 months leading up to the 28 June 2022 landslide (red star) compared to long-term (1990–2022) mean daily temperature (gray)

observations from news articles. In the following paragraphs, times reported for video-based observations are based on cell phone timestamps and are assumed to be accurate to the nearest minute. Times reported for seismic signals are corrected for seismic wave travel times as described in the “Methods” section and are likely accurate to within a few seconds.

There were signs that the slope was starting to mobilize for hours prior to the main slope failure. The eyewitnesses, who were frequent visitors to the area, observed that the slope was much more active than normal on the day of the landslide (Butzer 2022; Chen 2022). A series of videos from the hours before the main slide shared by one eyewitness (J. Fullerton, written comm., 2023) show

a progression from individual boulders dislodging and rolling down the slope below the Two Towers around 3 p.m. MDT (about 1.5 h prior to failure) to dozens of boulders and smaller rocks rolling simultaneously down different parts of the front of the slope around 3:36 p.m. MDT (about an hour before failure). This widespread buildup in surficial activity implies that marginally stable surface debris was responding to changes in the slope configuration likely due to slow sliding that was occurring at depth. Given that the closest seismic station was about 30 km away, we could not detect these smaller early rock falls in the seismic record.

Just prior to 4:30 p.m. MDT, the climbers sensed that activity was picking up. An eyewitness told us he was in the middle of a climb when his friends started yelling, and he felt the boulder he was on start vibrating. The group ran away to an area about 200–300 m directly in front of the slope where they felt they were far enough away to be safe (J. Fullerton, oral comm., 2023). One of the other climbers started filming the mobilization of the landslide from this location at about 4:30 p.m. MDT (Mondragon 2022). In the video, we can see the right-most of the Two Towers sink into the deforming slope, accompanied by a cascade of rocks of a variety of sizes rolling down the face of the frontal slope amongst thin flows of finer material. The entire slope begins to visibly move very slowly beneath this surface activity. This episode appears to last at least 30–40 s until the video cuts off. In the seismic record, there is a very subtle ~30-s vibration starting around 4:31:13 pm MDT (22:31:13 UTC) that may be associated with this initial period of activity, although the signal is certainly not clear enough to be identified as such on its own (Fig. 2a,  $t \sim 40$  s, labeled “Landslide?”).

The main landslide occurred a few minutes later. The entire slope started to rapidly accelerate towards the eyewitnesses, and they saw the snowfield detach and collapse (J. Fullerton, oral comm., 2023; Butzer 2022; Chen 2022). This occurred around 4:34 p.m. MDT, and the start of the main landslide was captured in a later part of the posted video compilation (Mondragon 2022). The climbers fled, becoming engulfed in a cloud of dust and debris but remained unharmed (J. Fullerton, oral comm., 2023). We estimated that the time at which they stop filming and run is about the same time that a park visitor at Lake Haiyaha started filming. That visitor’s video was shared on local news broadcasts (9news.com 2022). The main landslide is already underway at the start of this second video. This video shows the entire slope (extending up to the top of the source area and including a clear silhouette of the Two Towers about two-thirds of the way down) rapidly translating downslope relatively coherently until the towers rotate forward, and the entire slide becomes enveloped in dust. The top of the Two Towers is still visible above the dust and appears to stop somewhat abruptly. We estimated the velocity from the video to be  $5.4 \pm 1.0$  m/s (19 km/h) using the dimensions of the Two Towers for scale (see Online Resource 1 for details). This timeline of events is coincident with the buildup in seismic energy at the onset of the main seismic signal, which began to gradually emerge from the noise at 4:33:16 p.m. MDT (22:33:16 UTC), peaked at 4:34:25 (22:34:25 UTC), and then faded back into the noise by about 4:35:20 p.m. MDT (22:35:20 UTC) (Fig. 2a, labeled “Main landslide”). Although the total signal duration was about 2 min, the most energetic part of the signal, which we assume is associated with the most energetic part of the sliding motion that is caught on video, lasts about one minute. The signal reaches its highest amplitudes toward the end of the record,

after which the amplitudes rapidly drop and fade out. This is consistent with the relatively abrupt stop of the Two Towers visible in the video. The towers moved  $\sim 206$  m horizontally (Fig. 3d), which we estimate to be about  $\sim 245$  m along-slope, yielding rough average velocity estimates of 2–4 m/s if we assume the seismic duration spans the entire sliding episode. This estimate is slower than the velocity estimated from the video earlier (5.4 m/s), but this is expected because it also includes the initial acceleration from 0 m/s, which is not visible in the video.

Another energetic but smaller failure occurred several minutes after the main one according to the climbers. In this failure, they saw a crack in one of the displaced towers widen and then the tower rolled. This failure was not caught on video (J. Fullerton, oral comm., 2023). A faint seismic signal occurs at 4:42:21 p.m. MDT (22:42:11 UTC, not shown) that may be associated with the tower roll, although it is only visible in the record at one station due to noise in the records at other stations.

In the midst of this sequence of events, the seismic data show a small earthquake-like signal at 4:32:05 pm MDT (22:32:05 UTC) (Fig. 2a, labeled ‘Blast’). This occurred about a minute after the start of the seismic signal of the first sliding episode that was caught on video, but just over a minute prior to the onset of the main landslide. The signal has clear P-wave arrivals and strong surface wave energy implying a shallow, but impulsive source. We located the signal using the USGS National Earthquake Information Center’s location protocols (Patton et al. 2016) with the western U.S. velocity model (Herrmann et al. 2011) and estimated a local magnitude following the methods of Bormann and Dewey (2012). The signal was small; we estimated a local magnitude of  $M_{1.4}$ —events of that small size are rarely felt—and the seismic location, although uncertain, was within a few kilometers of the landslide (USGS 2022c). Given the time and location coincidence, we initially thought this signal was related to the landslide initiation process and thus investigated

further. However, after additional investigation detailed in Online Resource 1, we ultimately confirmed with the Chimney Hollow Reservoir construction project that the source was actually a blast associated with the construction of a new reservoir located about 36 km east of the landslide (Fig. 2b).

This blast likely did not cause the landslide, given that the resulting shaking was very weak and that the blast occurred after the landslide was already moving. The timing is likely a coincidence. Seismic station MCSU is about the same distance away from the blast as the landslide is, so we used the blast signal at MCSU to estimate the peak ground acceleration (PGA) at the location of the slide to be about 0.001% g. This is orders of magnitude lower than the lowest PGA levels known to trigger landslides during earthquakes (2–8% g, Jibson and Harp (2016)). However, given that the landslide accelerated somewhat dramatically almost immediately after the blast, it raises a question about whether the behavior of a landslide that is already actively moving could be accelerated by such a weak level of shaking. There are many examples in the literature where minor dynamic stress perturbations related to processes like ocean, Earth, and atmospheric tides, hydrologic loading, and minor shaking from distant earthquakes have influenced the behavior of glaciers, landslides, and faults (e.g., Thomas et al. 2012; Hill et al. 1993; Allstadt and Malone 2014; Schulz et al. 2009). Addressing the question of whether the blast on June 28, 2022, contributed to the acceleration of the Chaos Canyon landslide is beyond the scope of this paper but could be a topic for a future modeling study.

### Landslide characteristics

In this section, we summarize and interpret field and remote sensing observations of the landslide and its behavior during and following the main event on June 28, 2022. These observations

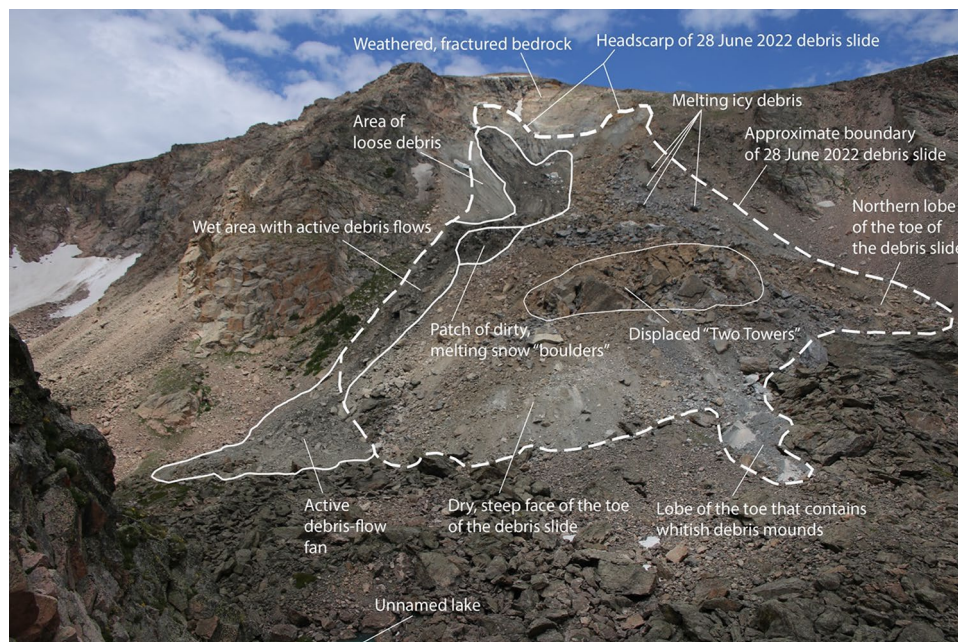


**Fig. 5** The June 28, 2022, debris slide with main features labeled. Horizontal distance from the middle of headscarp to the middle of toe is about 585 m. Photo taken from location d on Fig. 1 on July 15, 2022, by Jeff Coe/USGS

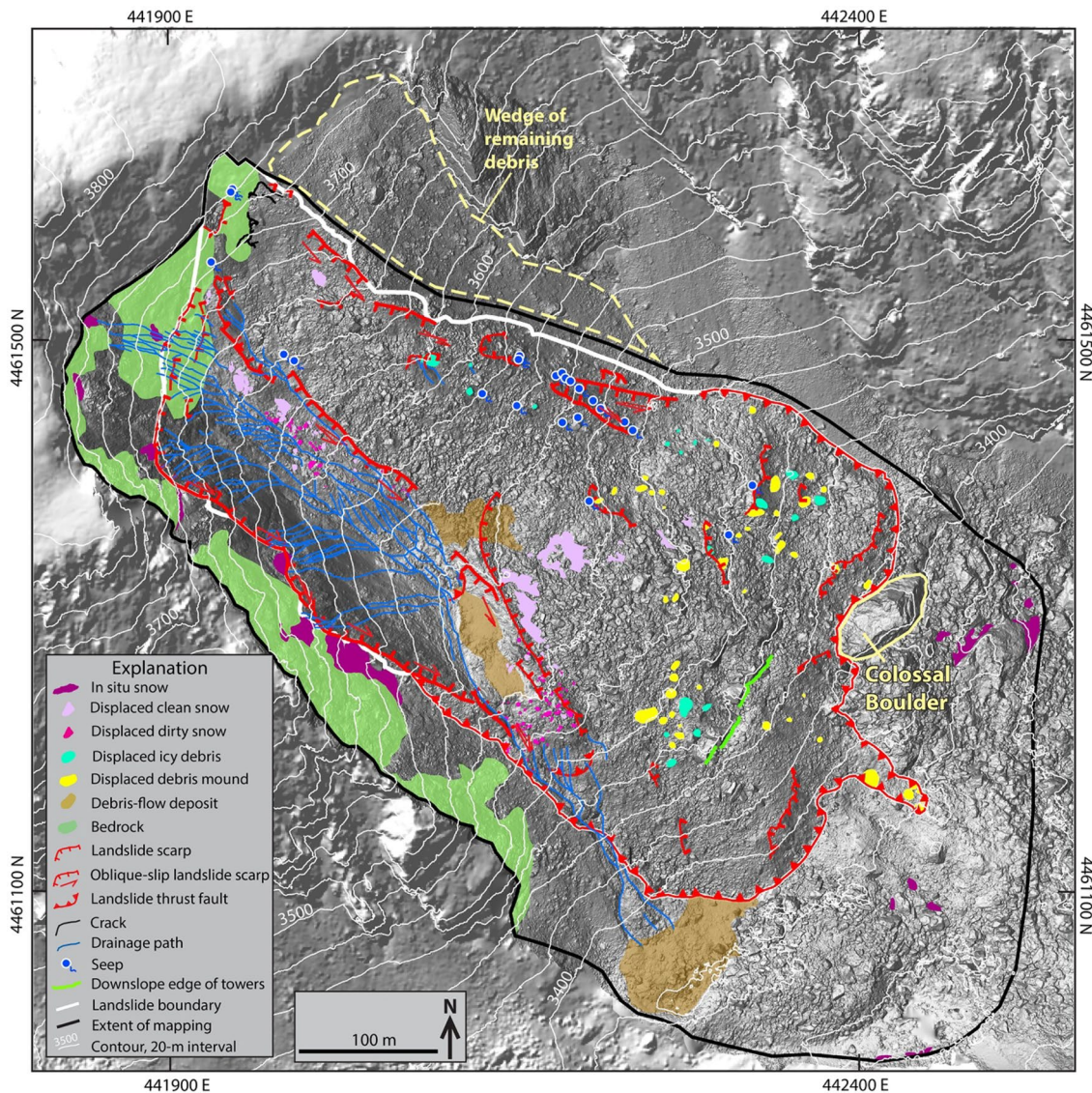


**Fig. 6** Map showing landslide structures, geology, and hydrology. Mapping was done at a scale of 1:500 using orthophotos and a shaded-relief DEM from the July 15, 2022, UAV mission. UAV-derived DEM hillshade is shown in areas inside the mapping extent boundary (thick black line), pre-event 1-m lidar data hillshade is shown in areas outside of the mapping extent boundary. Some landslide scarps and thrust faults form the boundary of the landslide and therefore overlap with the white landslide boundary line. Coordinates shown are UTM zone 13N

provide insights into landslide material, geometry, movement mechanisms, and constraints for forecasting future hazards at the site. An annotated overview photo of the landslide (Fig. 5) is accompanied by a detailed map of landslide structures, geology, and hydrology (Fig. 6) that was interpreted primarily based on a high-resolution (3-cm) orthophoto derived from the July 15, 2022, UAV photos.

Although it was unsafe to directly access the landslide during our field visit, photos and UAV imagery show that the June 28 landslide consisted of a wide range of grain sizes, from building-sized (~5–25 m) boulders to finer grained materials. Grain sizes were potentially as small as silt or even glacial flour, indicated by the milky aqua blue color of downstream water bodies such as Lake Haiyaha following the landslide (Fig. S9b). Landslide

material composed of such mixtures of grain sizes is generally referred to as debris (Hung et al. 2014). Very little to no bedrock was displaced, but bedrock forms the boundary of the west and south flanks of the June 28 landslide (Fig. 6) and is exposed as part of the basal slip surface near the headscarp (dashed outlined area, Fig. 7b). The material, visible slip surface, and the video that showed the landslide moving relatively coherently (9news.com 2022) at a peak velocity around 5 m/s, led us to classify the main June 28 landslide primarily as a debris slide. However, some internal deformation and intergranular motion is obvious in a comparison between pre- and post-event satellite images (e.g., Fig. 3b, d). This implies the slide was starting to grade into more of a granular flow, but did not ultimately become a faster, more flow-like debris avalanche, as is common for large debris slides



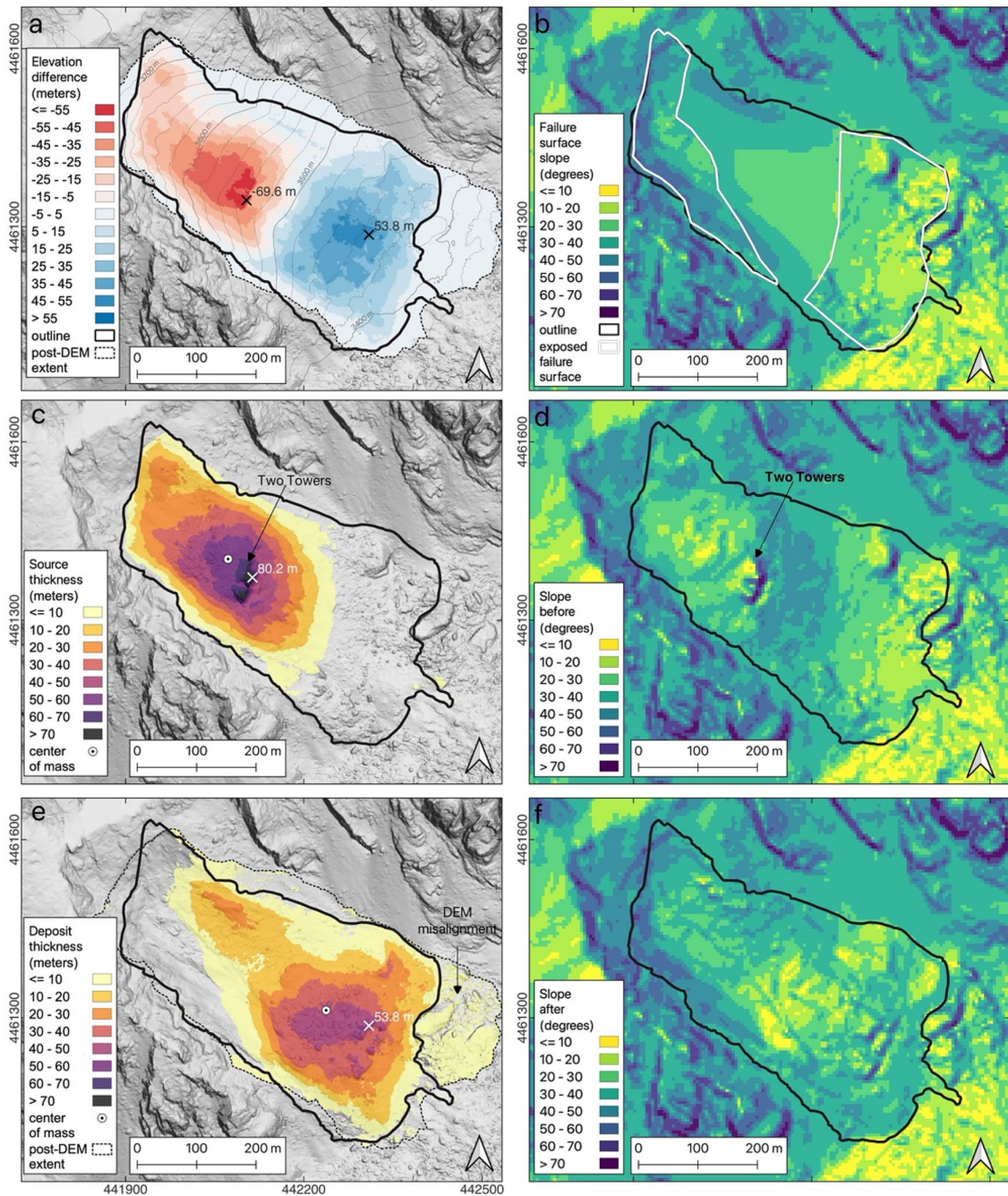


**Fig. 7** Elevation change, thickness estimates used to make volume estimates, and slope maps. **a** Elevation change caused by the landslide relative to the 2020 pre-event lidar DEM. Thin gray lines delineate the contours of the interpolated sliding surface used to derive the thickness plots in the following panels. **b** Slope of the interpolated failure surface. White polygons indicate the areas of the pre- and post-event DEMs assumed to represent the exposed sliding surface for interpolation. **c** Source thickness estimates overlain on the pre-event DEM and **d** slope of the pre-event DEM. **e** Deposit thickness estimates overlain on the post-event DEM and **f** slope of the post-event DEM. Areas with a thickness less than 0.1 m are masked in panels **c** and **e**, and non-zero thicknesses outside the landslide outline (thick solid line) but within the post-event DEM extent (thin dotted line) are due to errors in the alignment of the pre- and post-event DEM. Slopes were calculated at 5-m resolution. Coordinate reference system NAD83(2011)/UTM zone 13 N

(Hung et al. 2014). Instead, it came to a stop upon encountering the Chaos Canyon rock glacier on the floor of the canyon, where the toe of the June 28 debris slide overrode this boulder-rich material, forming a well-defined thrust fault (Fig. 6). The rock glacier

slopes are less steep in this area, but not flat (Fig. 7d). Part of the northern part of the toe abutted against a boulder known as “Colossal Boulder” with a long dimension of about 85 m (Fig. 6). The face of the toe is steep, with a median slope angle of  $\sim 35^\circ$

(Fig. 7f). A small, thin, elongated tongue of deposits about 70 m long and 15 m wide protrudes from the main toe (Figs. 5 and 6).

In situ and displaced patches of snow provided a guide to the location of the western and southern landslide boundaries, which were less clear than the other edges, allowing us to delineate the landslide boundaries (Fig. 6). The total map area of the landslide footprint is 154,000 m<sup>2</sup>. Our interpolation of the 3D failure surface (contours in Fig. 7a) and differencing that surface from the pre- and post-DEMs allowed us to examine the characteristics of the landslide source and deposits separately (Fig. 7c, e). The source has a map area of ~88,000 m<sup>2</sup> and a maximum vertical thickness of about 80 m, which occurred directly below the Two Towers (Fig. 7c). Our best estimate of the total volume of the source area is  $2.13 \times 10^6$  m<sup>3</sup> with a standard deviation (std) of  $0.12 \times 10^6$  m<sup>3</sup>. The deposits have a map area of ~122,000 m<sup>2</sup>, a maximum thickness of 54 m (Fig. 7e), and an estimated volume of  $2.09 \times 10^6$  m<sup>3</sup> (std  $0.12 \times 10^6$  m<sup>3</sup>). Lower-bound volume estimates from fitting a linear rather than slightly curving sliding surface yield  $1.85 \times 10^6$  m<sup>3</sup> and  $1.81 \times 10^6$  m<sup>3</sup> for source and deposits, respectively. The similarity of the volume estimates of the source and deposits implies that very little to no bulking occurred.

Elevations at the head and toe of the landslide, and the landslide travel distance, can be used as an index of mobility using the common vertical drop height/horizontal travel distance (*H/L*) ratio (e.g., Heim 1932; Hungr et al. 2005). The highest elevation of the headscarp is 3760 m, the lowest point of the deposits is 3380 m (*H* = 380 m) and the horizontal travel distance between the highest and lowest points (*L*) is ~700 m, yielding an *H/L* of 0.54 (28° reach angle). Using the source and deposit thickness distributions (Fig. 7) and assuming a constant density, we can also estimate the *H/L* of the landslide center of mass (*H/L*<sub>cm</sub>). *H/L*<sub>cm</sub> is less subjective and is a closer approximation of the effective coefficient of friction but harder to estimate for many events (Hsü 1975; Hungr et al. 2005). The center of mass moved 188 m horizontally and dropped 107 m (Fig. 7c, e), giving *H/L*<sub>cm</sub> = 0.57 (30° reach angle) and a slope-parallel displacement of 216 m. However, since the pre-event lidar was collected in 2020 and the landslide moved ~40 m horizontally between that time and just prior to the main event (Fig. 3), the *H/L*<sub>cm</sub> represents the aggregate of that motion. The Two Towers, in contrast, moved farther than the center of mass, reflecting the internal deformation that occurred. The Two Towers centroid moved about 206 m horizontally during the main event relative to its position in an image taken 1 week prior (Fig. 3c). After correcting the pre-event Two Towers centroid elevation for the ~40 m horizontal displacement that occurred between the 2020 pre-event lidar DEM and June 21, 2022 (Fig. 3c), using the slope of the failure surface below (~28°; Fig. 7b), we obtain a vertical drop of ~132 m. This equates to a slope-parallel displacement of the Two Towers of ~245 m during the June 28, 2022, event.

At an *H/L* of 0.54, the 2022 landslide had anomalously low mobility for its size when compared to an empirical mobility-volume relationship trained on a set of historical *H/L* data we found to be most similar in style and setting to Chaos Canyon: subaerial non-volcanic landslides (Hayashi and Self 1992). The Hayashi and Self (1992) relationship predicts an *H/L* of 0.42 for the volume of the Chaos Canyon landslide, with an estimated 95% uncertainty range (see Online Resources 1) of 0.35–0.52 (Fig. S6 inset). The *H/L* index for the 2022 landslide is just above this range indicating lower mobility than expected.

Just upslope from the Two Towers is a 50–70-m wide band where dozens of blocks of melting icy debris were scattered across the surface of the deposit in early July 2022 (Fig. 6). They are most visible in the July 2, 2022, satellite image, in which they appear as angular blocks 3–15 m long with melt rings around their boundaries (Fig. 8a, c). By the time of the July 13 satellite image, most of these well-defined blocks have melted and disintegrated into dry debris mounds (Fig. 8b, d). All indications are that melting occurred rapidly. An oblique photo taken on July 5, 2022, from Lake Haiyaha shows many of these melting blocks visible as wet spots (Fig. S9a). In comparison, by July 15, 2022, only a few of these spots were still visibly melting (Fig. 5). We hypothesize that these blocks of icy debris originated in the area upslope from the Two Towers that Achuff (2001) mapped as a rock glacier (Fig. 1). Some of this frozen debris was fractured and exposed in blocks at or near the surface during the landslide and began to rapidly melt and disintegrate into mounds. Such mounds of conical debris, known as molards, have long been observed in landslide deposits in periglacial environments (e.g., Goguel and Pachoud 1972). Molards have been hypothesized to form as blocks of frozen debris displaced in landslides that are initiated in response to permafrost melt (e.g., Milana 2016) and have been observed in deposits from glacier detachments that originated in permafrost terrain (Jacquemart et al. 2022). However, until the publication of Morino et al. (2019), there were few direct observations of the process of formation in landslides. The Chaos Canyon slide adds another example of their formation.

The most prominent and puzzling molards are the white and light gray mounds that sit in the elongate tongue at the toe of the deposits (Fig. 5). Two of the most distal mounds are visible in their original frozen form in an eyewitness video taken about half an hour after the landslide (J. Fullerton, written comm., 2022). The orientation of thick bands of alternating gray and white material in these boulder-like blocks matches the orientation of those colors in the melted molards (Fig. 9a). The blocks had already started disintegrating by the July 2, 2022, satellite image, but they still have defined edges and visible melt rings. By the time of our field visit on July 15, they had melted into dry conical debris mounds with a small central core of coherent material remaining (Fig. 9b, c). Our mapping shows a trail of these blocks down the front of the toe that is aligned with the elongated tongue. This trail appears to originate near a low point between blocks of the displaced Two Towers, behind which most of the other frozen blocks remained (Fig. 8). This trail implies that the frozen blocks of debris rolled down the face of the toe through this low point between the Two Towers (possibly associated with the 4:42:21 p.m. MDT post-event tower roll described earlier), forming the elongated tongue. The composition of the blocks appears to be a finer grained, lighter-color material than most of the other slide deposits, but its composition is unknown because it was unsafe to directly visit the mounds at the time of our July 15 field visit.

Normal and oblique-slip fault scarps created by movement on June 28 (Fig. 6) indicate that there were internal slides within the overall debris slide. Some internal slides are located along the north flank of the June 28 debris slide. Of particular interest are two arcuate-shaped internal scarps and downslope oblique-slip lateral scarps near the northern flank of the debris slide where active seeps were located on 15 July (Fig. 6). Given that blocks of permafrost

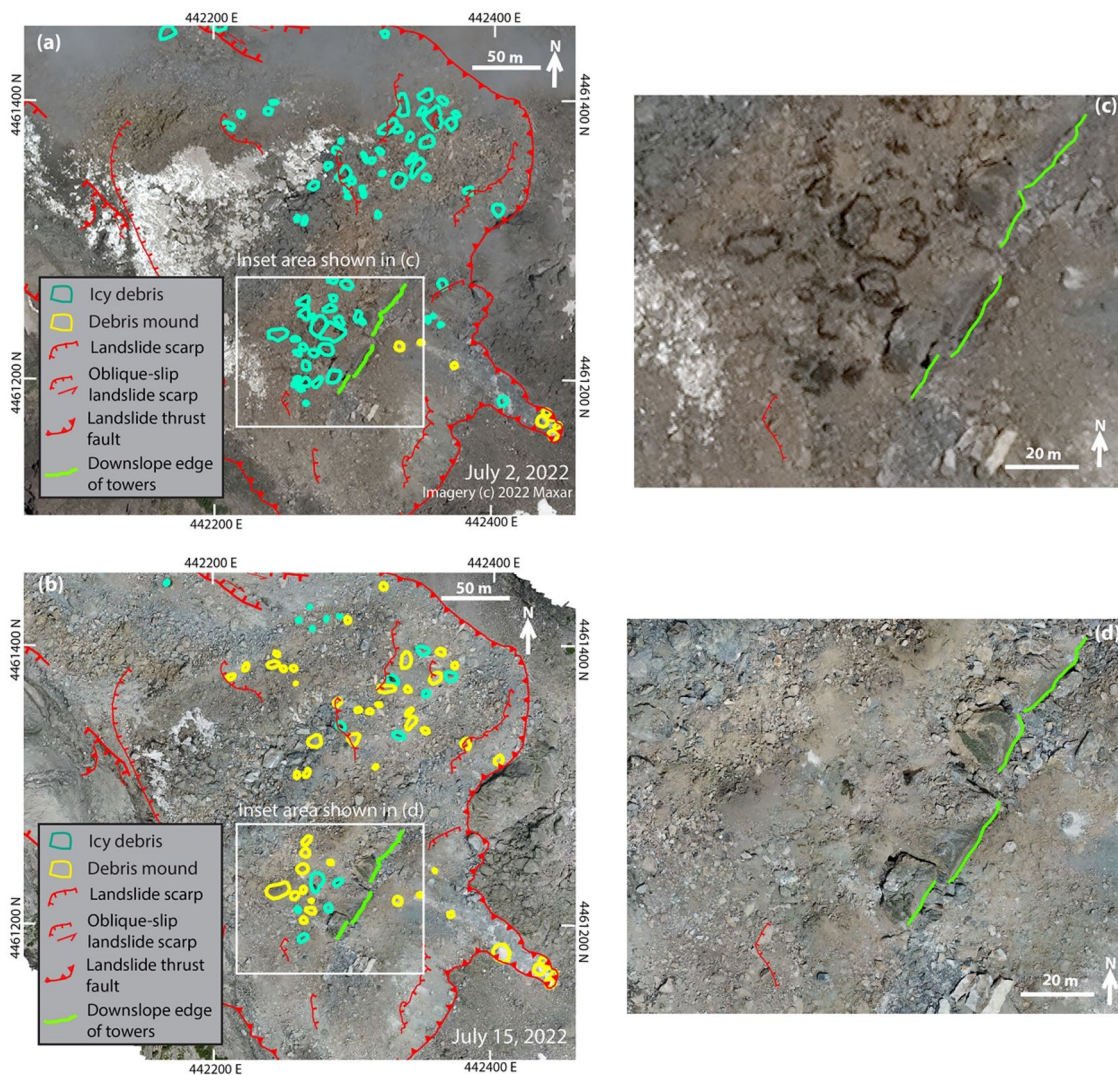


**Fig. 8** Images and maps showing the evolution of icy debris (green polygons) to dry debris mounds (yellow polygons) on the lower half of the June 28, 2022, debris slide. **a** Maxar image and map from July 2, 2022. **b** UAV image and map from July 15, 2022. Panels **c** and **d** show close-ups of inset areas labeled in **a** and **b**, respectively, without the debris outlines. Note that with warm summer temperatures, most patches of icy debris from July 2, 2022, have evolved into dry debris mounds by July 15, 2022. Coordinates shown are UTM zone 13 N

originated in this area, as evidenced above, we believe these seeps are likely related to melting icy debris that was exposed when material slid downslope from these areas. Other than these seeps, the north and central parts of the landslide appeared relatively dry and inactive by the time of our field visit.

In contrast, a more prominent area of internal movement along the south side of the landslide remained wet and active for weeks, fed by melting snow and possible bedrock seeps from the southern part of the headscarp. This area is also where the snowfield typically remained late into the summer as other parts melted, and likely had the largest snow thickness. We know from eyewitnesses that the snowfield collapsed with the debris slide during the main event, and blocks of snow from the snowfield are visible in the deposits in a post-event video all the way down the front of the toe south of the Two Towers (J. Fullerton, written comm. 2023). In the same video, taken ~ 22 min after the main event, the southern

lateral scarp and southern part of the headscarp are visible in the background and it appears that large patches of the upper snowfield were displaced by just a few tens of meters and remained otherwise largely intact in the source area (Fig. 9a).

The eyewitnesses also saw water coming from “behind the Two Towers” after the landslide (J. Fullerton, oral comm. 2023), which we interpret to mean from the southern part of the headscarp because it appeared very wet during our field visit more than 2 weeks later. Fed by surface water and melting snow, flows of snow, and debris traveled down this south edge of the landslide. By July 2, a distinct ~ 50-m by ~ 350-m-long channel had developed. Within this channel, wet debris interspersed with blocks of clean snow are visibly working their way down to a flatter area where the distal portions of the snowfield that failed in the main event came to rest. One of these subsequent flows of a slurry of snow and debris was captured on video on July 8, 2022, by hiker on a ridge above

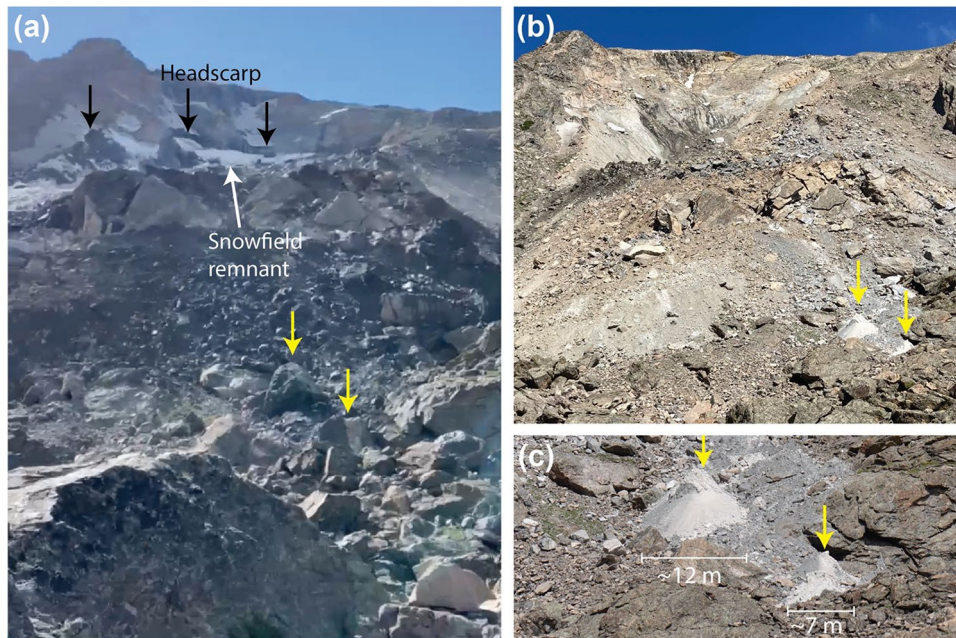


**Fig. 9** Evidence of molar evolution: **a** screenshot from a video taken from near location **b** in Fig. 1 about 23 min after the main landslide, video screenshot courtesy of Jeremy Fullerton. Yellow arrows indicate two distinctive frozen blocks of permafrost that appear boulder-like that rolled down the debris slide. **b** The same two blocks in a photo taken on July 15, 2022, that have melted and degraded into conical mounds of debris (molards). **c** A close up of the same two mounds. Photos **b** and **c** taken from location **c** in Fig. 1 (Kate Allstadt/USGS)

(Morris 2022). By the time of our next clear view of the deposits in a satellite image from July 13, and the UAV orthophoto from July 15, most of the snowfield remnants were gone and the activity had evolved from these larger flows of snow and wet debris, to smaller debris flows coming down numerous small channels. This channel network is mapped in Fig. 6. By July 15, a “dam” of boulders of snow had also accumulated at the end of the original channel, about 200 m from the toe, behind which debris flow deposits were actively accumulating at the time of our visit (debris flow deposit upslope from magenta “displaced dirty snow” in Fig. 6; Online Resource 1 Fig. S10). Surface water was flowing down the south side of the toe below this dam of snow, occasionally entraining material and forming debris flows that were actively forming the southern-most debris flow deposit. The flows were stopping in a depression adjacent to the southern edge of the landslide toe (Fig. 6). During our field visit, we observed two debris flows in these channels along the south side, as well as numerous individual rock falls and rolling rocks over a period of about 3 h. The northern most debris-flow deposit (Fig. 6) formed sometime between July 2 and July 13 and was not receiving fresh material during our visit on July 15. Based on previous research, it is common for debris flows to occur following failures of permafrost-rich debris slopes like rock glaciers (e.g., Bodin et al. 2012, 2017; Delaloye et al. 2013; Deline et al. 2015; Marcer et al. 2020; Janke and Bolch 2022).

A photo of the upper part of the landslide taken by a hiker from a ridge above on August 9 2022 (P. Miller, written comm., 2022; Online Resource 1 Fig. S11), shows that by this date, all remnants of the snow have melted, only the southernmost corner of the headscarp was still actively seeping water, and the flow channels had largely coalesced into a single channel flowing along the southernmost edge of the deposit. The entirety of the landslide appears

dry in the next available high-resolution (~1-m) BlackSky satellite image acquired on October 16, 2022, snow began to accumulate by the end of the month, and by mid-November the landslide was covered with snow for the winter.

## Discussion

### Future hazard in Chaos Canyon

In their request for technical assistance from the USGS, NPS was especially interested in any information we could provide regarding possible ongoing hazards to help inform their decision making. In this section, we briefly summarize the information and analysis we provided NPS in response to this request based on the information presented above, historical precedent, and simple runout analyses. More details are included in Online Resource 1.

The area downslope from the June 28 landslide remains hazardous. Small debris flow and rock fall activity continues. Throughout the summer and fall of 2022, NPS staff received daily to weekly reports from hikers that they heard activity coming from the area above Lake Haiyaha and some visual reports of additional smaller slide activity in the source area. The NPS received fewer reports of additional activity from park visitors in the spring and summer of 2023. Small rock falls and debris flows will likely continue but rates may be tapering off as the slope equilibrates to its new configuration, although activity patterns will likely be influenced by intensity and duration of snowmelt and summer thunderstorms. During spring months, years that have above normal snowpack, or years with a condensed period of rapid snowmelt, could favor more and possibly larger failures because there would be ample time to generate pore pressure deep within the deposit. Summer thunderstorms on the other hand would be most likely to generate smaller

debris flows at the site, most likely along the southern edge of the slide where debris flows were active following the June 2022 catastrophic slide event. A rain-on-snow event following a winter with high snowpack, and during rapid melting in an anomalous spring warm period, would likely be a worst-case scenario for generating rapid slide movement.

One area of concern with regards to future larger failures is an adjacent wedge of debris remaining in the cirque, north of the source area of the June 28 landslide (Fig. 6). Assuming mean vertical thicknesses of 5 to 15 m and an area of  $\sim 19,000 \text{ m}^2$ , the wedge could have a volume of  $\sim 100,000\text{--}300,000 \text{ m}^3$ . The seeps we mapped along the southern edge of this wedge indicate permafrost may also be present in this debris (Fig. 6). There is also a small fracture along the top of this wedge (Online Resource 1 Fig. S11), although we do not have enough information to determine if it has widened since the 28 June landslide occurred. It is possible that this wedge of material, which has been debuttressed and exposed to warmer temperatures along its southern edge, could subsequently fail.

Another concern would be the remobilization of a substantial portion of the  $\sim 2 \text{ million m}^3$  2022 debris-slide deposits. The deposits are still relatively steep: the median slope angle of the surface of the deposits,  $34^\circ$ , (range  $0.1\text{--}83^\circ$ ), is steeper than the effective friction angle of the main landslide ( $30^\circ$ , based on  $H/L_{\text{cm}} = 0.57$ ). Also, we observed fresh cracks at the interface between bedrock and debris (thin black lines at northernmost part of Fig. 6). Although these cracks could be due to settlement, they could also indicate that the debris slide moved between June 28 and July 15, and may continue to move in the future.

A worst-case scenario would be the rapid remobilization of the entirety of the deposits. This is unlikely given the material is now in a more stable configuration: the median slope of the slip surface below the material decreased from  $33^\circ$  pre-event to  $27^\circ$  afterwards. However, landslides at the same location and in the same material can reactivate differently with greatly different mobilities and consequences (e.g., see La Conchita and Oso landslides, Jibson 2005; Iverson et al. 2015). For example, the introduction of more water into the system, an impulsive force from the collapse of additional material upslope, and/or strong ground motion could result in a landslide that is more mobile and flow-like than the 28 June landslide. Alternatively, slower, creep-like movement is also possible and would be less hazardous.

One major concern during the response to this event was whether additional failures or remobilizations could reach areas farther down the canyon that are frequented by climbers and hikers. To examine this possibility, we conducted some simple runout modeling using SHALTOP, a depth-averaged 3D shallow-water granular flow model (Bouchut et al. 2003; Bouchut and Westdickenberg 2004; Mangeney et al. 2007; Lucas et al. 2014; Peruzzetto et al. 2021). Given limited information about internal landslide material and grain sizes, we used the simplest rheological law, the Coulomb friction law, and calibrated the runout to historical mobility (H/L) measurements from similar landslide types and volumes (Hayashi and Self 1992). This process and results are described in detail in Online Resource 1. In summary, we found that the mobility is limited because depressions south and east of the toe in the irregular, undulating, topography of the Chaos Canyon rock glacier act as sinks for much of the material (Fig. S6). Only at the upper mobility range of the historical data does the leading edge of the

simulated flow reach an area informally known as “the Meadow,” where climbers sometimes congregate (Fig. S6c).

Mobility might be further limited by factors that are not accounted for in the modeling such as the extremely large grain size (car- and house-sized boulders) at the surface of the Chaos Canyon rock glacier and the lack of a well-defined surface channel. Flow channelization and the liquefaction and entrainment of deposits along the flow path are all factors that increase landslide mobility (e.g., Iverson et al. 2011; Coe et al. 2016; Collins and Reid 2019; Pudasaini and Krautblatter 2021) and neither are likely in Chaos Canyon. However, we note that there are considerable uncertainties. For example, there are alternate approaches to estimating runout distances that predict higher mobilities (Online Resource 1, Fig. S7). In addition, although the surface of the landslide deposits is coarse, there may be finer grained material within the landslide mass (e.g., composition of the molards in the elongated tongue) that could allow for more mobile, flow-like behavior than what we are considering in the historical mobility datasets chosen for this analysis.

### Broader implications

To our knowledge, the Chaos Canyon debris slide is the first documented landslide in the continental United States (i.e., the lower 48 states) where permafrost was not only exposed by slide movement but also strongly suspected to play a role in the initiation of the landslide by melting and contributing to increased pore pressures within the slide mass. Prior to the Chaos Canyon event, even the presence of permafrost in the lower 48 states, in locations other than in the cores of rock glaciers, was controversial because it had not been directly observed. In the last decade or so, with increasing air temperatures worldwide, permafrost degradation has been suspected in landslide initiation (in both rock and debris) in many other parts of the world, including Canada, Alaska, Iceland, Greenland, Norway (including Svalbard), and the European Alps (e.g., Ravanel and Deline 2011; Fischer et al. 2013; Coe et al. 2018; Sæmundsson et al. 2018; Friele et al. 2020; Kuhn et al. 2021; Svennevig et al. 2022; Penna et al. 2023). The presence of permafrost at Chaos Canyon implies that permafrost may be present in other higher altitude areas in the western USA and that these areas are not immune to landslides induced by melting permafrost.

Given that the Chaos Canyon landslide was moving for many years prior to catastrophic failure as temperatures warmed, our results indicate that improved meteorological and landslide monitoring at high elevations in Colorado, as well as in other parts of the world, would be helpful in detecting and understanding alpine landslides induced by permafrost degradation. Rangwala and Miller (2012) highlighted the need for more climatic monitoring in mountains, noting that, for example, nearly all US National Weather Service and SNOTEL sites are at elevations less than 3500 m, and those above 3000 m are limited. Yet, these higher elevations are where permafrost is most likely in the western United States (e.g., Janke 2005a). Other high-altitude permafrost areas in comparable climatic and geomorphic settings to Chaos Canyon may be susceptible to landsliding in the near future or could already be moving. Systematic remote monitoring for slope deformation, for example, through the use of satellite-based synthetic aperture radar (SAR)

or optical image-correlation techniques (e.g., Kääb 2002; Stumpf et al. 2017; Lu and Kim 2021), might be feasible (although not trivial to implement). This would be most beneficial for areas with a high volume of human traffic or that contain critical infrastructure. The joint US National Aeronautics and Space Administration (NASA) and Indian Space Research Organisation (ISRO) Synthetic Aperture Radar Mission (NISAR, (<https://nisar.jpl.nasa.gov/>) and its planned automated surface deformation products might help bring this within reach. NISAR is currently scheduled to launch in 2024 and observe much of the Earth's surface about every 6 days. However, the detection of slope deformation alone is not enough information to accurately forecast hazard because many slopes move slowly for many years without failing catastrophically. The transition from slow sliding to runaway acceleration is still an area of active research (e.g., Lacroix et al. 2020).

### Conclusions

The Chaos Canyon landslide was sourced in glacial debris and talus that contained permafrost. The source area may even have been a rock glacier, although we do not have enough evidence at present to say for certain (e.g., whether it was creeping due to internal ice deformation). Much of the  $\sim 2$  million  $m^3$  of debris that would eventually fail rapidly started sliding slowly about two decades ago, around the same time that rising annual mean temperatures at the elevation of the slope started to exceed  $0^\circ\text{C}$ . As temperatures further increased, sliding rates accelerated, and during the spring and summer snowmelt season, on June 28, 2022, at 4:33:16 p.m. MDT, the landslide failed catastrophically. The mass, which was up to 80-m thick, reached peak velocities around  $\sim 5$  m/s, and came to rest upon reaching the Chaos Canyon rock glacier, a relict or fossil rock glacier characterized by car- and house-sized boulders. Permafrost that was in the source material during the landslide broke into large blocks of frozen debris that were visible in the deposits, but the blocks were short-lived. The icy debris melted into dry conical mounds of debris called molards within a few weeks. Melting remnants of a snowfield that previously crowned the debris slope, along with continued seasonal snowmelt from adjacent areas, fed flows of snow, and debris that evolved into debris flows flowing frequently down the southern edge of the deposits for several weeks after 28 June.

Seismic recordings, and eyewitness videos and reports allowed for the reconstruction of the rapid failure sequence in nearly unprecedented detail. The sequence was composed of two main sliding episodes within minutes of each other that were energetic enough to be recorded seismically (and potentially a third  $\sim 9$  min later), although the second, main event, during which most of the displacements occurred, was by far the most energetic. Even prior to those three energetic episodes, eyewitness accounts indicated that surface activity was elevated (e.g., rolling and falling rocks), implying the sliding actually started several hours prior to catastrophic failure. The co-occurrence of a nearby small (M1.4-equivalent) blast in the midst of the mobilization sequence, immediately prior to slide acceleration into a rapid, catastrophic failure, raises interesting questions about the influence of minor transient stresses on Earth systems teetering on the edge of instability.

The occurrence of this landslide, its drawn-out decade-long acceleration sequence, and its likely association with rising

temperatures and melting permafrost raise the question of whether there are other similar slopes in Rocky Mountain National Park, nearby parts of the Front Range, or other similar alpine areas in many locations throughout the world, where similar processes may already be underway.

### Acknowledgements

We acknowledge Jeremy Fullerton (eyewitness), Matthew Morriss, Bill Schulz, Jon Achuff, Katy Barnhart, Joel Smith, Rob Chase, Jack Wood, Eric Bilderback, Mason Einbund, Marc Peruzzetto, and Antoine Lucas for contributing information and insight to this study. We thank Rex Baum and an anonymous reviewer for comments that greatly improved the manuscript and Mike Lukens, Andrew Eaton, Rydell Stottlemeyer, and Nadine Reitman for assisting in the fieldwork.

### Author contribution

Data collection and processing were performed by K. A., J. C., F. R., S. E., and L. B. Geospatial data and landslide analysis was conducted by K. A., J. C., and E. C. K. A., W. Y., J. P., and J. B. conducted the seismic analysis. K. A., A. M., and J. C. conducted runout modeling. The first draft of the manuscript was written by K. A., J. C., and E. C., and all authors commented on previous versions and approved the final manuscript.

### Funding

This work was funded by the US Geological Survey and National Park Service. Anne Mangeney was funded by the Digital Twin for GEophysical extremes (DT-GEO) and the Doctoral Network EnvSeis.

### Data availability

The post-event DEM, high-resolution orthophoto, and original UAV images are available for download from the USGS ScienceBase data release associated with this article (Rengers et al. 2023) at <https://doi.org/10.5066/P9ZQY3G>. The pre-event lidar is available for download from USGS ScienceBase at <https://www.sciencebase.gov/catalog/item/620de575d34e6c7e83baa0d8>. Bear Lake SNOTEL data used in this study (last accessed 03 January 2023) is available from the USDA Natural Resources Conservation Service at <https://wcc.sc.gov.usda.gov/nwcc/site?sitenum=322>. Seismic data used in this study are available for download from the IRIS Data Management Center at <http://service.iris.edu/iriswv/>.

### Declarations

**Disclaimer** Any use of trade, firm, or product names is for descriptive purposes only and does not imply endorsement by the US Government.

**Conflict of interest** The authors declare no competing interests.

**Open Access** This article is licensed under a Creative Commons Attribution 4.0 International License, which permits use, sharing, adaptation, distribution and reproduction in any medium or format, as long as you give appropriate credit to the original author(s) and the source, provide a link to the Creative Commons licence, and indicate if changes were made. The images or other third party

material in this article are included in the article's Creative Commons licence, unless indicated otherwise in a credit line to the material. If material is not included in the article's Creative Commons licence and your intended use is not permitted by statutory regulation or exceeds the permitted use, you will need to obtain permission directly from the copyright holder. To view a copy of this licence, visit <http://creativecommons.org/licenses/by/4.0/>.

## References

- 9news.com (2022) Hallett Peak rockslide in Rocky Mountains National Park captured by hiker. <https://www.9news.com/video/sports/outdoors/hallett-peak-rockslide-in-rocky-mountains-national-park-captured-by-hiker/73-2c76e565-9ab1-4cf4-a985-39ea7e229fad>. Accessed 24 Feb 2023
- Achuff JM (2001) Preliminary map of glacier complexes and firnfields of Rocky Mountain National Park. Rocky Mt Natl Park Glacier Firnfield Monit Program
- Agisoft (2022) Agisoft Metashape Professional (Version 1.8.3) (software). <https://www.agisoft.com/downloads/installer/>
- Albuquerque Seismological Laboratory (ASL)/USGS (1990) United States National Seismic Network. Int. Fed. Digit. Seismogr. Netw. <https://doi.org/10.7914/SN/US>
- Allen SK, Gruber S, Owens IF (2009) Exploring steep bedrock permafrost and its relationship with recent slope failures in the Southern Alps of New Zealand. *Permafir Periglac Process* 20:345–356. <https://doi.org/10.1002/ppp.658>
- Allstadt KE, Malone SD (2014) Swarms of repeating stick-slip icequakes triggered by snow loading at Mount Rainier volcano. *J Geophys Res Earth Surf* 119:2014JF003086. <https://doi.org/10.1002/2014JF003086>
- Allstadt KE, Matoza RS, Lockhart AB et al (2018) Seismic and acoustic signatures of surficial mass movements at volcanoes. *J Volcanol Geotherm Res* 364:76–106. <https://doi.org/10.1016/j.jvolgeores.2018.09.007>
- Anderson LR, Keaton JR, Saarinen TF, Wells WG (1984) The Utah landslides, debris flows, and floods of May and June 1983. National Academy Press
- Bodin X, Krysielki J-M, Iribarren Anacona P (2012) Recent collapse of rock glaciers two study cases in the Alps and in the Andew. In: Extended abstracts 12th Congress INTERPRAEVENT. Grenoble, France, p 3
- Bodin X, Krysielki J-M, Schoeneich P et al (2017) The 2006 collapse of the Bérard Rock Glacier (Southern French Alps). *Permafir Periglac Process* 28:209–223. <https://doi.org/10.1002/ppp.1887>
- Bormann P, Dewey JW (2012) The new IASPEI standards for determining magnitudes from digital data and their relation to classical magnitudes. *New Man Seismol Obs Pract* 2 NMSOP-2 1–44. [https://doi.org/10.2312/GFZ.NMSOP-2\\_IS\\_3.3](https://doi.org/10.2312/GFZ.NMSOP-2_IS_3.3)
- Bouchut F, Westdickenberg M (2004) Gravity driven shallow water models for arbitrary topography. *Commun Math Sci* 2:359–389
- Bouchut F, Mangeney-Castelnaud A, Perthame B, Vilotte J-P (2003) A new model of Saint Venant and Savage-Hutter type for gravity driven shallow water flows. *Comptes Rendus Math* 336:531–536. [https://doi.org/10.1016/S1631-073X\(03\)00117-1](https://doi.org/10.1016/S1631-073X(03)00117-1)
- Braddock WA, Cole JC (1990) Geologic map of Rocky Mountain National Park and vicinity, Colorado. US Geol Surv Misc Investig Ser Map I-1973:2. <https://doi.org/10.3133/i1973>
- Butzer S (2022) "We were essentially running for our lives": four climbers flee rockslide in Rocky Mountain National Park. In: [denver7.com/news/local-news/rockslide-reported-on-southside-of-hallett-peak-in-rocky-mountain-national-park](https://www.denver7.com/news/local-news/rockslide-reported-on-southside-of-hallett-peak-in-rocky-mountain-national-park). Accessed 13 Mar 2023
- Cannon S, Gartner JE, Holland-Sears A, Thurston BM (2003) Debris-flow response of basins burned by the 2022 Coal Seam and Missionary Ridge Fires, Colorado. In: Boyer DD, Santi PM, Rogers P (eds) *Engineering geology in Colorado, contributions, trends, and case histories*. p 30
- Chen HYT (2022) Massive rockslide destroys classic boulders in Rocky Mountain National Park. In: *Climbing*. <https://www.climbing.com/news/rockslide-destroys-classic-boulders-rocky-mountain-national-park/>. Accessed 20 Jan 2023
- Chleborad AF (1998) Use of air temperature data to anticipate the onset of snowmelt-season landslides. US Geol Surv Open-File Rep 98–124. <https://doi.org/10.3133/ofr98124>
- Coe JA, Kean JW, Godt JW et al (2014) New insights into debris-flow hazards from an extraordinary event in the Colorado Front Range. *GSA Today* 24:4–10
- Coe JA, Baum RL, Allstadt KE et al (2016) Rock-avalanche dynamics revealed by large-scale field mapping and seismic signals at a highly mobile avalanche in the West Salt Creek valley, western Colorado. *Geosphere* 12:607–631. <https://doi.org/10.1130/GES01265.1>
- Coe JA, Bessette-Kirton EK, Geertsema M (2018) Increasing rock-avalanche size and mobility in Glacier Bay National Park and Preserve, Alaska detected from 1984 to 2016 Landsat imagery. *Landslides* 1–15. <https://doi.org/10.1007/s10346-017-0879-7>
- Collins BD, Reid ME (2019) Enhanced landslide mobility by basal liquefaction: the 2014 State Route 530 (Oso), Washington, landslide. *GSA Bull* 132:451–476. <https://doi.org/10.1130/B35146.1>
- Colorado Geological Survey (2016) Colorado Geological Survey Seismic Network. Int. Fed. Digit. Seismogr. Netw. <https://doi.org/10.7914/SN/C0>
- Colton RB, Holligan JA, Anderson LW, Patterson PE (1976) Preliminary map of landslide deposits in Colorado. IMAF. <https://doi.org/10.3133/i964>
- Davis PT (1988) Holocene glacier fluctuations in the American Cordillera. *Quatern Sci Rev* 7:129–157. [https://doi.org/10.1016/0277-3791\(88\)90003-0](https://doi.org/10.1016/0277-3791(88)90003-0)
- Delaloye R, Morard S, Barbois C, et al (2013) Rapidly moving rock glaciers in Mattertal. In: *Jahrestagung der Schweizerischen Geomorphologischen Gesellschaft*
- Deline P, Gruber S, Delaloye R et al (2015) Chapter 15 - Ice loss and slope stability in high-mountain regions. In: Shroder JF, Haeblerli W, Whiteman C (eds) *Snow and Ice-Related Hazards, Risks, and Disasters*. Academic Press, Boston, pp 521–561
- Duncan JM, Fleming RW, Patton FD (1986) Report of the Thistle Slide Committee to State of Utah, Department of Natural Resources, Division of Water Rights. US Geol Surv Open-File Rep 86–505. <https://doi.org/10.3133/ofr86505>
- EDF R&D (2023) CloudCompare (v 2.13.0) [GPL software]. <http://www.cloudcompare.org/>
- Fischer L, Huggel C, Käab A, Haeblerli W (2013) Slope failures and erosion rates on a glacierized high-mountain face under climatic changes. *Earth Surf Process Landf* 38:836–846. <https://doi.org/10.1002/esp.3355>
- Friele P, Millard TH, Mitchell A et al (2020) Observations on the May 2019 Joffre Peak landslides, British Columbia. *Landslides* 17:913–930. <https://doi.org/10.1007/s10346-019-01332-2>
- Godt JW, Coe JA (2007) Alpine debris flows triggered by a 28 July 1999 thunderstorm in the central Front Range, Colorado. *Geomorphology* 84:80–97. <https://doi.org/10.1016/j.geomorph.2006.07.009>
- Goguel J, Pachoud A (1972) Géologie et dynamique de l'écroulement du Mont-Granier, dans le Massif de Chartreuse, en novembre. *Bull Bur Rech Géologiques Minières* 3:29–38
- Hadley JB (1964) The Hebgen Lake, Montana, earthquake of August 17, 1959. US Geol Surv Prof Pap 435:242. <https://doi.org/10.3133/pp435>
- Haeblerli W, Wegmann M, Vonder Mühl D (1997) Slope stability problems related to glacier shrinkage and permafrost degradation in the Alps. *Eclogae Geol Helvetiae* 90:407–414
- Hayashi JN, Self S (1992) A comparison of pyroclastic flow and debris avalanche mobility. *J Geophys Res Solid Earth* 97:9063–9071. <https://doi.org/10.1029/92JB00173>
- Heim A (1932) *Bergsturz und menschenleben*. Fretz & Wasmuth
- Herrmann RB, Benz H, Ammon CJ (2011) Monitoring the earthquake source process in North America. *Bull Seismol Soc Am* 101:2609–2625. <https://doi.org/10.1785/0120110095>

- Hill DP, Reasenber PA, Michael A et al (1993) Seismicity remotely triggered by the magnitude 7.3 Landers, California, earthquake. *Science* 260:1617–1623. <https://doi.org/10.1126/science.260.5114.1617>
- Hoffman MJ, Fountain AG, Achuff JM (2007) 20th-century variations in area of cirque glaciers and glacierets, Rocky Mountain National Park, Rocky Mountains, Colorado, USA. *Ann Glaciol* 46:349–354. <https://doi.org/10.3189/172756407782871233>
- Hsü KJ (1975) Catastrophic debris streams (Sturzstroms) generated by rockfalls. *Geol Soc Am Bull* 86:129. [https://doi.org/10.1130/0016-7606\(1975\)86%3c129:CDSSGB%3e2.0.CO;2](https://doi.org/10.1130/0016-7606(1975)86%3c129:CDSSGB%3e2.0.CO;2)
- Hungr O, Corominas J, Eberhardt E (2005) Estimating landslide motion mechanism, travel distance and velocity. In: *Landslide Risk Management*. CRC Press
- Hungr O, Leroueil S, Picarelli L (2014) The Varnes classification of landslide types, an update. *Landslides* 11:167–194. <https://doi.org/10.1007/s10346-013-0436-y>
- International Union of Geological Sciences Working Group on Landslides (IUSS) (1995) A suggested method for describing the rate of movement of a landslide. *Bull Int Assoc Eng Geol - Bull Assoc Int Géologie Ing* 52:75–78. <https://doi.org/10.1007/BF02602683>
- Iverson RM, Reid ME, Logan M et al (2011) Positive feedback and momentum growth during debris-flow entrainment of wet bed sediment. *Nat Geosci* 4:116–121. <https://doi.org/10.1038/ngeo1040>
- Iverson RM, George DL, Allstadt KE et al (2015) Landslide mobility and hazards: implications of the 2014 Oso disaster. *Earth Planet Sci Lett* 412:197–208. <https://doi.org/10.1016/j.epsl.2014.12.020>
- Jacquemart M, Welty E, Leopold M et al (2022) Geomorphic and sedimentary signatures of catastrophic glacier detachments: a first assessment from Flat Creek. *Alaska Geomorphology* 414:108376. <https://doi.org/10.1016/j.geomorph.2022.108376>
- Janke JR (2005a) The occurrence of alpine permafrost in the Front Range of Colorado. *Geomorphology* 67:375–389. <https://doi.org/10.1016/j.geomorph.2004.11.005>
- Janke JR (2005b) Long-term flow measurements (1961–2002) of the Arapaho, Taylor, and Fair Rock Glaciers, Front Range, Colorado. *Phys Geogr* 26:313–336. <https://doi.org/10.2747/0272-3646.26.4.313>
- Janke JR (2005c) Modeling past and future alpine permafrost distribution in the Colorado Front Range. *Earth Surf Process Landf* 30:1495–1508. <https://doi.org/10.1002/esp.1205>
- Janke JR (2007) Colorado Front Range rock glaciers: distribution and topographic characteristics. *Arct Antarct Alp Res* 39:74–83. <https://www.jstor.org/stable/4139118>
- Janke J, Frauenfelder R (2008) The relationship between rock glacier and contributing area parameters in the Front Range of Colorado. *J Quat Sci* 23:153–163. <https://doi.org/10.1002/jqs.1133>
- Janke JR, Bolch T (2022) 4.06 — Rock glaciers. In: Shroder J (Jack) F (ed) *Treatise on Geomorphology* (Second Edition). Academic Press, Oxford, pp 75–118
- Jibson RW (2005) Landslide hazards at La Conchita. *California US Geol Surv Open-File Rep* 2005–1067:12. <https://doi.org/10.3133/ofr20051067>
- Jibson RW, Harp EL (2016) Ground motions at the outermost limits of seismically triggered landslides. *Bull Seismol Soc Am* 106:708–719. <https://doi.org/10.1785/0120150141>
- Kääb A (2002) Monitoring high-mountain terrain deformation from repeated air- and spaceborne optical data: examples using digital aerial imagery and ASTER data. *ISPRS J Photogramm Remote Sens* 57:39–52. [https://doi.org/10.1016/S0924-2716\(02\)00114-4](https://doi.org/10.1016/S0924-2716(02)00114-4)
- Kuhn D, Torizin J, Fuchs M et al (2021) Back analysis of a coastal cliff failure along the Forkastningsfjellet coastline, Svalbard: Implications for controlling and triggering factors. *Geomorphology* 389:107850. <https://doi.org/10.1016/j.geomorph.2021.107850>
- Lacroix P, Handwerker AL, Bièvre G (2020) Life and death of slow-moving landslides. *Nat Rev Earth Environ* 1:404–419. <https://doi.org/10.1038/s43017-020-0072-8>
- Lee WT (1923) Peneplains of the Front Range and Rocky Mountain National Park, Colorado. *US Geol Surv Bull* 730-A: <https://doi.org/10.3133/b730A>
- Lu Z, Kim J (2021) A framework for studying hydrology-driven landslide hazards in Northwestern US using satellite InSAR, precipitation and soil moisture observations: Early results and future directions. *Geo-Hazards* 2:17–40. <https://doi.org/10.3390/geo-hazards2020002>
- Lucas A, Mangeney A, Ampuero JP (2014) Frictional velocity-weakening in landslides on Earth and on other planetary bodies. *Nat Commun* 5:3417. <https://doi.org/10.1038/ncomms4417>
- Madole RF (1976) Glacial Geology of the Front Range of Colorado. In: Mahaney WC (ed) *Quaternary Stratigraphy of North America*. Dowden, Hutchinson & Ross, pp 297–318
- Mangeney A, Bouchut F, Thomas N, et al (2007) Numerical modeling of self-channeling granular flows and of their levee-channel deposits. *J Geophys Res Earth Surf* 112:. <https://doi.org/10.1029/2006JF000469>
- Marcier M, Ringsø Nielsen S, Ribeyre C et al (2020) Investigating the slope failures at the Lou rock glacier front, French Alps. *Permafrost Periglacial Process* 31:15–30. <https://doi.org/10.1002/ppp.2035>
- McGrath D (2022) Blowing in the wind: The glaciers of Colorado. *Mt Geol* 59:229–238. <https://doi.org/10.31582/rmag.mg.59.3.229>
- Milana JP (2016) Molards and their relation to landslides involving permafrost failure. *Permafrost Periglacial Process* 27:271–284. <https://doi.org/10.1002/ppp.1878>
- Mondragon W [@williammondragon] (2022) Landslide [Video]. <https://www.instagram.com/reel/CfZjN9KPoWr/>. Accessed 23 Jan 2023
- Morino C, Conway SJ, Sæmundsson Þ et al (2019) Molards as an indicator of permafrost degradation and landslide processes. *Earth Planet Sci Lett* 516:136–147. <https://doi.org/10.1016/j.epsl.2019.03.040>
- Morris M [@RockIceandSnow] (2022) The views today got exciting [video]. <https://twitter.com/RockIceandSnow/status/1545609735042486277?s=20&t=djiZYA5oSwAgugPFD6Mjsw>
- Outcalt SI, Benedict JB (1965) Photo-interpretation of two types of rock glacier in the Colorado Front Range, U.S.A. *J Glaciol* 5:849–856. <https://doi.org/10.3189/S0022143000018918>
- Patterson K (2022) Rocky Mountain National Park closes Chaos Canyon area due to rockslide - Rocky Mountain National Park (U.S. National Park Service). <https://www.nps.gov/romo/learn/news/rocky-mountain-national-park-closes-chaos-canyon-area-due-to-rockslide.htm>. Accessed 20 Jan 2023
- Patton JM, Guy MR, Benz HM, et al (2016) Hydra—The National Earthquake Information Center’s 24/7 seismic monitoring, analysis, catalog production, quality analysis, and special studies tool suite. *US Geol Surv Open-File Rep* 2016–1128:. <https://doi.org/10.3133/ofr20161128>
- Patton AI, Rathburn SL, Capps DM (2019) Landslide response to climate change in permafrost regions. *Geomorphology* 340:116–128. <https://doi.org/10.1016/j.geomorph.2019.04.029>
- Penna IM, Magnin F, Nicolet P et al (2023) Permafrost controls the displacement rates of large unstable rock-slopes in subarctic environments. *Glob Planet Change* 220:104017. <https://doi.org/10.1016/j.gloplacha.2022.104017>
- Peruzzetto M, Mangeney A, Bouchut F, et al (2021) Topography curvature effects in thin-layer models for gravity-driven flows without bed erosion. *J Geophys Res Earth Surf* 126:e2020JF005657. <https://doi.org/10.1029/2020JF005657>
- Pudasaini SP, Krautblatter M (2021) The mechanics of landslide mobility with erosion. *Nat Commun* 12:6793. <https://doi.org/10.1038/s41467-021-26959-5>
- Rangwala I, Miller JR (2012) Climate change in mountains: a review of elevation-dependent warming and its possible causes. *Clim Change* 114:527–547. <https://doi.org/10.1007/s10584-012-0419-3>
- Ravanel L, Deline P (2011) Climate influence on rockfalls in high-Alpine steep rockwalls: the north side of the Aiguilles de Chamonix (Mont Blanc massif) since the end of the ‘Little Ice Age.’ *The Holocene* 21:357–365. <https://doi.org/10.1177/0959683610374887>
- Rengers FK, McGuire LA, Coe JA et al (2016) The influence of vegetation on debris-flow initiation during extreme rainfall in the northern Colorado Front Range. *Geology* 44:823–826. <https://doi.org/10.1130/G38096.1>
- Rengers FK, Reitman NG, Brady LR, et al (2023) UAV imagery and digital elevation model for the debris slide in Chaos Canyon, 28 June 2022, Rocky Mountain National Park, Colorado. *US Geol Surv Data Release*. <https://doi.org/10.5066/P9ZQQY3G>



- Richmond GM (1960) Glaciation of the East Slope of Rocky Mountain National Park, Colorado. GSA Bull 71:1371–1382. [https://doi.org/10.1130/0016-7606\(1960\)71\[1371:GOTESO\]2.0.CO;2](https://doi.org/10.1130/0016-7606(1960)71[1371:GOTESO]2.0.CO;2)
- Sæmundsson Þ, Morino C, Helgason JK et al (2018) The triggering factors of the Móafellshyrna debris slide in northern Iceland: intense precipitation, earthquake activity and thawing of mountain permafrost. *Sci Total Environ* 621:1163–1175. <https://doi.org/10.1016/j.scitotenv.2017.10.111>
- Schulz WH, Kean JW, Wang G (2009) Landslide movement in southwest Colorado triggered by atmospheric tides. *Nat Geosci* 2:863–866. <https://doi.org/10.1038/ngeo659>
- Schuster RL, Highland LM (2001) Socioeconomic and environmental impacts of landslides. US Geol Surv Open-File Rep 01–0276. <https://doi.org/10.3133/ofr01276>
- Stumpf A, Malet J-P, Delacourt C (2017) Correlation of satellite image time-series for the detection and monitoring of slow-moving landslides. *Remote Sens Environ* 189:40–55. <https://doi.org/10.1016/j.rse.2016.11.007>
- Svennevig K, Hermanns RL, Keiding M et al (2022) A large frozen debris avalanche entraining warming permafrost ground—the June 2021 Assapaat landslide, West Greenland. *Landslides* 19:2549–2567. <https://doi.org/10.1007/s10346-022-01922-7>
- Thomas AM, Bürgmann R, Shelly DR, et al (2012) Tidal triggering of low frequency earthquakes near Parkfield, California: implications for fault mechanics within the brittle-ductile transition. *J Geophys Res Solid Earth* 117. <https://doi.org/10.1029/2011JB009036>
- U.S. Geological Survey (USGS) (2022a) USGS Global Visualization Viewer (GloVis). <https://glovis.usgs.gov/>. Accessed 26 Feb 2023
- U.S. Geological Survey (USGS) (2022b) USGS 1 Meter 13 x44y447 CO\_DRCOG\_2020\_B20. US Geol Surv Data Release. <https://www.sciencebase.gov/catalog/item/620de575d34e6c7e83baa0d8>
- U.S. Geological Survey (USGS) (2022c) M 1.4–10 km NE of Grand Lake, Colorado. In: USGS Earthq. Hazards Program. <https://earthquake.usgs.gov/earthquakes/eventpage/us6000hynr/executive>. Accessed 20 Feb 2023
- White SE (1976) Rock glaciers and block fields, review and new data. *Quat Res* 6:77–97. [https://doi.org/10.1016/0033-5894\(76\)90041-7](https://doi.org/10.1016/0033-5894(76)90041-7)
- Wieczorek GF, Lips EW, Ellen SD (1989) Debris flows and hyperconcentrated floods along the Wasatch Front, Utah, 1983 and 1984. *Environ Eng Geosci* xxvi:191–208. <https://doi.org/10.2113/gseegeosci.xxvi.2.191>

Supplementary Information The online version contains supplementary material available at <https://doi.org/10.1007/s10346-023-02179-4>.

**Kate E. Allstadt** (✉) · **Jeffrey A. Coe** · **Elaine A. Collins** · **Francis K. Rengers** · **William L. Yeck**

U.S. Geological Survey Geologic Hazards Science Center, Golden, CO, USA

**Kate E. Allstadt**  
Email: kallstadt@usgs.gov

**Anne Mangeney**  
Université Paris Cité, Institut de Physique du Globe de Paris, CNRS, F-75005 Paris, France

**Anne Mangeney**  
Institut Universitaire de France, Paris, France

**Scott M. Esser**  
Rocky Mountain National Park, National Park Service, Estes Park, CO, USA

**Jana Pursley** · **John J. Bellini**  
U.S. Geological Survey National Earthquake Information Center, Golden, CO, USA

**Lance R. Brady**  
U.S. Geological Survey National Uncrewed Systems Office, Denver, CO, USA